Available online at www.sciencedirect.com

ScienceDirect

Physics Procedia 83 (2016) 135 – 146

Physics Procedia

9th International Conference on Photonic Technologies - LANE 2016

Influence of an angular hatching exposure strategy on the surface roughness during picosecond laser ablation of hard materials

Christian Daniel[a,]*, Jannik Manderla[a], Sina Hallmann[a], Claus Emmelmann[a]

[a]Institute of Laser and System Technologies, Hamburg University of Technology, Hamburg 21073, Germany

Abstract

Innovative chip breakers for cutting tools made of very hard materials require laser ablation and demand a high quality regarding the manufactured surface. When processing materials such as polycrystalline cubic boron-nitride or tungsten carbide the surface roughness by laser ablation reaches S_a = 1,0-2,9 µm compared to S_a = 0,42 µm achieved by grinding. Therefore in the presented research the influence of the hatching exposure strategy on surface roughness during picosecond laser ablation of tungsten carbide is examined. The areal, layerwise ablation process is separated into its elements which are represented by intersection zones between single and multiple laser vectors. Thus two mechanisms of roughness formation are identified and described by model functions. Further the mechanisms are transferred to areal ablation in which surface roughness decreases due to improved hatching angles compared to a commonly used one of φ= 0°/90°. With this approach the roughness is reduced by approximately factor 2,0-3,5 to S_a = 0,82 µm. In conclusion guidelines are derived which present favorable settings for high quality laser ablation processes.

Peer-review under responsibility of the Bayerisches Laserzentrum GmbH

Keywords: picosecond laser ablation; hatching angle; surface roughness; hard materials; tungsten carbide

1. Introduction

Short- and ultrashort pulsed laser ablation of hard materials is used for manufacturing of geometries in the micrometer range for cutting tools, dental implants, injection molds or in post-processing and finishing of 3D-printed parts [1-4]. Furthermore laser processing by ultrashort laser radiation enhances the manufacturing of very small

* Corresponding author. Tel.: +49-40-484010-741 ; fax: +49-40-484010-999 .
E-mail address: christian.daniel@tuhh.de

Peer-review under responsibility of the Bayerisches Laserzentrum GmbH
doi:10.1016/j.phpro.2016.08.026

geometries for example for chip breakers in cutting tools from hard materials such as tungsten carbide (TC) or polycrystalline cubic boron nitride (PCBN) [5].

Chip breakers in cutting materials of high hardness are conventionally manufactured by grinding or electrical discharge machining (EDM). Nevertheless in these manufacturing methods the geometrical freedom is limited by the shape and size of the grinding wheels or electrodes and a critical heat affected zone (HAZ) is present [6]. Laser ablation, in contrast to the conventional methods, enables a non-contact, and thus force- and wear-free processing. The geometric diversity is significantly less subject to limitations and areas normally difficult to access can be machined. In this context laser ablation enhances innovative cutting tool designs which are able to realize new potential for improved chipping processes with higher cutting speeds and reduced tool wear when machining ultrahigh strength steels or titanium alloys.

For cutting tools and chip breakers from hard materials there occur high demands regarding the surface quality. Here conventional processes are still superior. While the surface roughness S_a of tungsten carbide after grinding amounts $S_a = 0{,}42$ µm the surface roughness by laser ablation reaches $S_a = 1{,}0\text{-}2{,}9$ µm when processing in axial direction of the laser beam. Nevertheless when a specifically tailored and adjusted surface roughness is required laser ablation is advantageous [2].

To further utilise the benefits offered by laser ablation the roughness needs to be reduced. The influence on the surface quality of laser parameters such as average power, pulse frequency, scan speed, focal position et cetera is described in multiple studies [7-10]. Besides by laser parameters the surface roughness is significantly influenced by the hatching exposure strategy. In this context the hatching angle becomes important to the eventual surface roughness of the chip breaker cavity.

During laser ablation voluminous geometries such as chip breakers are processed by a layerwise, areal material removal. In each layer the cross-sectional area is filled with parallel laser vectors and thus a constant track distance (*TD*) and pulse distance (*PD*) is maintained. The hatching angle describes the angle between laser vectors of two consecutive layers.

This research considers the central questions which quantitative influence of the hatching exposure strategy on the final surface roughness can be characterized and how the appearance of roughness through exposure strategies can be explained. Therefore the influence of specific hatching angles on the surface quality during picosecond laser ablation of hard materials is examined and affecting mechanisms of roughness formation are identified. Further the concluding question is answered which setting has to be applied as a favorable hatching angle for a high quality laser ablation process.

2. State of the art

The influence of an angular hatching exposure strategy on the surface roughness is only marginally analyzed. In recent studies during laser ablation with the objective to reduce the surface roughness of 3D-printed parts Campanelli et al. (2013) used a 45° hatching angle [10]. However, the angle was not varied further and in the analysis only laser parameters were taken into account as a factor of influence on roughness. During laser finishing of metallic materials Koch (2011) was applying a hatching angle on copper when working with a $t_p = 100 – 500$ ns pulsed $P = 16$ W Nd:YAG-Laser [11]. The process result was improved when following layers are not congruent. A congruence equates a hatching angle of $\varphi = 0°$. With an alternating hatching angle between each layer ($\varphi_n = 0°$ and $\varphi_{n+1} = 90°$) a roughness of $R_a = 3{,}3$ µm was achieved after ablation of $n = 10$ layers and with a hatching angle of $\varphi = 60°$ a roughness of $R_a = 2{,}5$ µm was measured. Koch (2011) assumes that the smaller the hatching angle the more homogenous the overlap of laser tracks and thus the higher the surface quality. At the $\varphi = 0/90°$ setting an oriented, microscopic structure was observed which affects the surface roughness. The structure was not present on the $\varphi = 60°$ setting in Kochs (2011) study. Nevertheless the examination of further angular settings is neglected and detailed mechanisms of roughness formation are not described.

Other technological approaches to reduce a surface roughness by laser processing can already realize a high surface quality. With laser polishing Rosa et al. (2015) were able to achieve a roughness of up to $S_a = 0{,}79$ µm and Temmler et al. (2011) could even reach $R_a < 0{,}1$ µm [12-13]. However this polishing process uses laser remelting. Material on the surface of workpieces is molten and a smooth surface is created by surface tension of the melt. Therefore the process is not feasible for materials with no distinguished melting point such as carbon-fiber-

reinforced plastic (CFRP) or materials with such a high melting point such as PCBN or TC that surrounding areas would be thermally damaged if the melting point is exceeded over a significantly longer duration than usual pulsewidths. Also it is not applicable for parts that allow no thermal impact, no microstructural change or no recast zone at all such as medical implants or aerospace parts .

Another approach to achieve a high surface quality from laser processes concentrates on the integration of sensor technology. The sensoric system is subject to gathering characteristic process data such as process radiation, acoustic emissions or distance between sensor and surface of the workpiece [14-15]. To take influence on the laser process the processing of sensor data and an according adaption of laser parameters is necessary. Therefore this approach requires complex and expensive hard- and software for an automatic control. To avoid an increase in cost of new ablation systems or an expensive and supplementary backfitting of industrially used ablation machines the present research establishes a fast and easy possibility to significantly improve surface quality with no additional expenses.

3. Experimental setup

3.1. Material

Investigations are carried out on a type KXF (K10-K40) carbide metal with a tungsten carbide (TC) content of 90 % and a cobalt-based binder to gain a basic understanding of the mechanisms of surface roughness formation. The average grain size is 0,7 µm, the density 14,4 g/cm3 and the Vickers Hardness *HV30* = 1.610. Laser ablation of the blanks starts on an original surface with a roughness of $S_{a,orig}$ = 0,42 µm processed by grinding.

3.2. Laser system and setup

The experiments were performed by use of a picosecond laser source which emits laser pulses with a pulsewidth of t_P = 10 ps and a wavelength of λ = 1.064 nm. The average power can be set up to P = 50 W and the repetition rate is adjustable from f = 400 – 1.000 kHz. The mechanical beam guiding system consists of three linear axes and two rotary ones for a maximum of geometric diversity. In addition, the beam deflection system provides three optical axes with a maximum scan field size of 70 mm x 70 mm in the x-y-plane. The focal length of the *F-Θ*-lens is 163 mm. After a parameter determination, following the methodical approach of Daniel et al. (2016) [7], the laser parameters are kept constant as shown in Table 1. In each layer the pulse-distance (*PD*) and the track-distance (*TD*), which define the distribution of following pulses, and the distance between parallel laser tracks are set to *PD* = 2 µm and *TD* = 6 µm. The scan speed is v_s = 1250 mm/s. Experimental results such as ablation depth, track width and dimensions of the intersection areas are measured using confocal microscopy.

Table 1. Fixed laser parameters.

Parameter	Pulsewidth	Average power	Repetition rate	Scan speed	Wavelength	Width of laser track / Focal diameter
Variable	t_p	P	f	v_s	λ	d_F
Value	10	17	1.000	1.250	1.064	34
Unit	ps	W	kHz	mm/s	nm	µm

3.3. Methodology

For the investigation on forming mechanisms of surface roughness a methodical approach was created. For the detailed analysis of the occurring mechanisms of surface roughness formation the areal, layerwise ablation process is separated into its elements which are represented by intersection zones between two as well as intersection zones between multiple laser vectors and the characteristic of cycle completion number is introduced (Figure 1). The aggregated observations are then merged in the areal ablation and development stages of roughness formation are examined. The results of all experiments allow for a conclusion about favorable settings for high quality laser ablation processes.

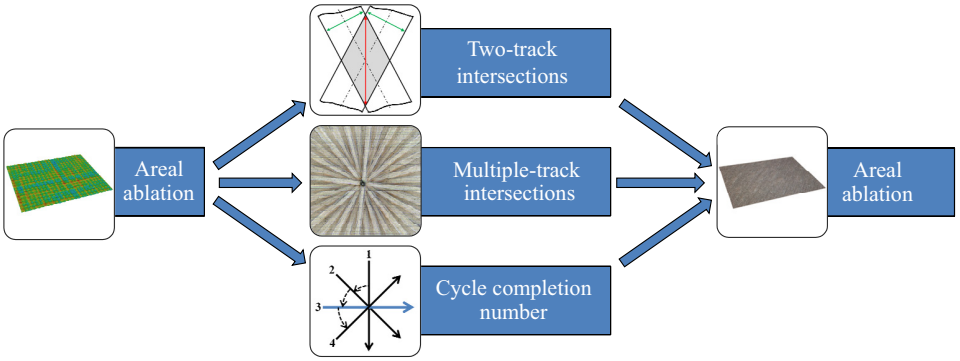

Fig. 1. Methodical approach.

For areal ablation the direction of the laser vectors for each layer is defined by the direction of the previous layer plus the hatching angle. A bidirectional exposure strategy where following laser vectors are directed contrary to each other was used during all experiments on areal ablation. For quantification of the surface roughness the arithmetical mean height S_a and the maximum height S_z within a definition area was measured according to ISO 25178 using a confocal microscope. Surface roughness was determined 6 times to ensure reproducibility and the average is displayed at each experiment. Due to the analogy of experimental results regarding S_a and S_z only S_a is depicted in the following analysis. Furthermore hatching angles from $\varphi = 0° – 180°$ behave equally to angles from $\varphi = 180° – 360°$ due to reasons of geometrical symmetry. The symmetry is exploited and therefore angles from $\varphi = 180° – 360°$ are neglected in the experimental approach.

4. Results and Discussion

4.1. Areal ablation and surface roughness depending on the hatching angle

To find general connections between the hatching angle and the surface roughness laser ablation at all integer hatching angles from $\varphi = 0° – 180°$ was performed. The number of ablated layers was $n = 360$ for each setting of hatching angle. Figure 2 shows the resulting surface roughness S_a depending on the hatching angle. The roughness of the ground, original surface is $S_{a,orig} = 0{,}42$ µm. All roughness values from ablation are achieved while keeping the setting of laser parameters from Table 1 constant. The average of all roughness values from ablation is $S_{a,aver} = 0{,}89$ µm. In contrast to the average roughness there occur single, exposed points that show a higher roughness than from the surrounding angular settings. A noticeable higher roughness can be observed e.g. at angles of $\varphi = 30°, 45°, 90°, 120°$ et cetera (Figure 2). Furthermore settings of hatching angles from $\varphi = 0° − 5°$ show a trend of decreasing roughness, coming from a high value, while angular settings from $\varphi = 175° − 180°$ show an increasing roughness.

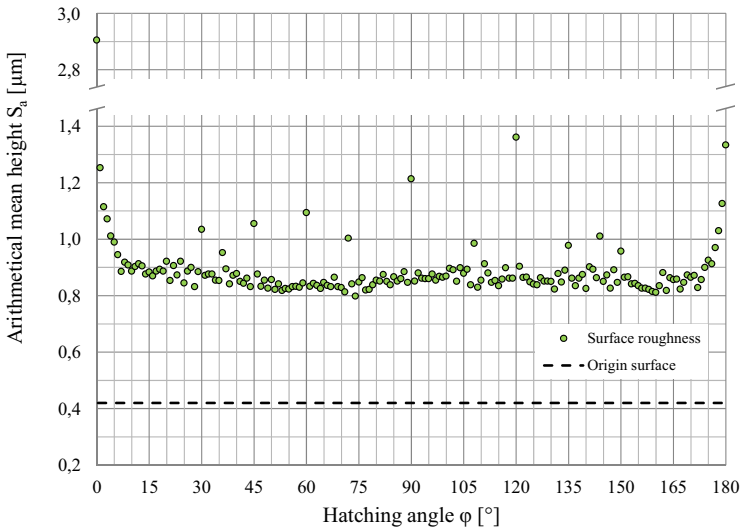

Fig. 2. Surface roughness depending on the hatching angle.

Due to the prior executed determination of laser parameters the mean surface roughness could already be set to a relatively low level of $S_{a,aver} = 0{,}89$ µm compared to ablation processes in common [2-4, 11]. While also the preliminary condition of the original surface influences the overall achievable roughness, when fluencies are not set up ideally an irregular ablation and a thus increased roughness can occur. Regarding the presence of an ultrashort ablation regime the energy penetration depth and optical penetration depth need to be taken into account. The ultra short condition is fulfilled when the energy penetration depth during the interaction of a laser pulse with the material is equal or smaller than the optical penetration depth. Energy penetration depth depends on the heat diffusion coefficient and the interaction time between the laser pulse and the material. Optical penetration depth is influenced by the absorption coefficient which itself is material and wavelength dependent [16]. With a wavelength of $\lambda = 1.064$ nm, a pulse width of $t_p = 10$ ps and a high thermal conductivity of K10-K40 tungsten carbide grade of $\kappa = 65 – 80$ W/mK the energy penetration depth is situated in the same range as the optical penetration depth [17]. Therefore the present ablation can be regarded as an optically dominated ablation process. Based on the preliminary parameter determination also a thermal influence by heat accumulation through pulse to pulse interaction was avoided and in an additional SEM analysis the absence of a relevant heat affected zone and resolidified melt was confirmed. A heat affected zone and resolidified melt would have increased the overall roughness level.

The fundamental question that arises from the present experiment is how the characteristic and the exposed values in Figure 2 can be explained. Therefore as described in Section 3.3, two fundamental experiments are created to clarify the behaviour of roughness formation.

4.2. Two-track intersection

On areas exposed with a hatching angle of $\varphi \in]\,0°, 180°[$ there occur intersections between laser tracks of subsequent ablation layers. The mathematical set excludes $\varphi = 0°$ and $\varphi = 180°$ due to no presence of intersection. From a microscopic point of view the intersections between laser vectors are not point-shaped but include a considerable area due to the width of laser tracks d_F. The intersection area A_{IA} is defined as the overlapping area of two laser tracks from two different layers (Figure 3). A_{IA} can be calculated from the intersection diagonal d_{IA} which is a function of laser track width d_F and hatching angle φ (1).

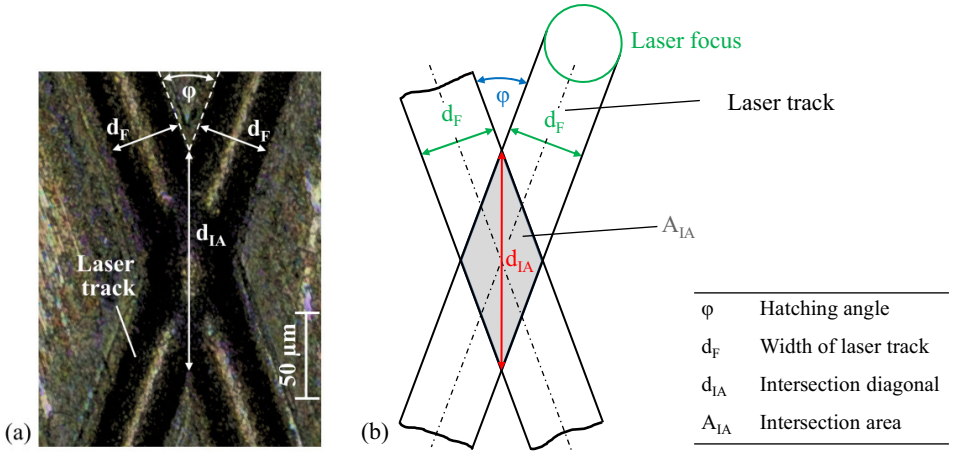

Fig. 3. Dimensions of a two-track intersection area (a) microscopic image; (b) schematic representation.

$$d_{IA} = \frac{d_F}{\sin(\frac{\varphi}{2})} \quad \forall\, \varphi \in]0,90\,] \;, \qquad d_{IA} = \frac{d_F}{\cos(\frac{\varphi}{2})} \quad \forall\, \varphi \in]90,180\,[\tag{1}$$

The objective of the examination on two-track intersection areas is to determine how the formation of surface roughness is influenced directly by intersection areas. Therefore a single laser track with orientation of $\varphi = 0°$ is ablated which is subsequently intersected with single laser tracks each orientated at the angles in Table 2. Laser track width is kept constant at $d_F = 34$ µm during all experiments. The choice of investigated angles is based on the results of the surface roughness experiment (Figure 2). Several angular settings where a high roughness occurs were examined ($\varphi = 1°, 2°, 3°, 4°, 30°, 45°, 60°, 72°, 90°, 120°, 179°$) complemented by settings with a low roughness ($\varphi = 39°, 125°$). A noticeable characteristic is that several angular settings with a high roughness represent integer dividers of 360° (Table 2). Nevertheless other settings also with a high roughness do not show this characteristic. Furthermore two regimes of integer dividers can be classified, those with a denominator ≥ 12 and those with a denominator < 12 (Table 2). This indicates that more than one mechanism may contribute to formation of roughness.

Table 2. Investigated hatching angles for two-track intersection.

Hatching angle φ [°]	1	2	3	4	30	39	45	60	72	90	120	125	179
Corresponding integer divider of 360° (if existent)	$\frac{360}{360}$	$\frac{360}{180}$	$\frac{360}{120}$	$\frac{360}{90}$	$\frac{360}{12}$	-	$\frac{360}{8}$	$\frac{360}{6}$	$\frac{360}{5}$	$\frac{360}{4}$	$\frac{360}{3}$	-	-
Surface roughness S_a [µm]	1,25	1,11	1,07	1,01	1,04	0,87	1,06	1,09	1,00	1,21	1,36	0,84	1,13

After execution of the experiments the intersection diagonal d_{IA} and ablation depth of intersection areas were measured for all hatching angles from Table 2. Additionally also depth of each single laser track was analysed and proved to be constant as expected ($\Delta z_{single} \approx 18$ µm). Further results show that the depth of track intersection areas ($\Delta z_{intersect} \approx 34$ µm) is 1,8 − 2,0 times higher than the depth of single laser tracks. Nevertheless the depth of intersection areas is independent of the hatching angle.

Regarding intersection diagonal Figure 4 shows a model function of the hatching angle. The values of the intersection diagonal strongly decrease for angles from $\varphi = 1° - 5°$, stay on a level of $d_{IA} < 200$µm for gaining hatching angles and strongly increase for angular settings from $\varphi = 175° - 179°$. Furthermore results from the experiment show a high correlation between the calculated and measured intersection diagonal (Figure 4) which means that also the corresponding intersection area can be calculated. Standard deviations for $d_{IA} < 200$µm ocurr in such a small range that they cannot be seen in Figure 4.

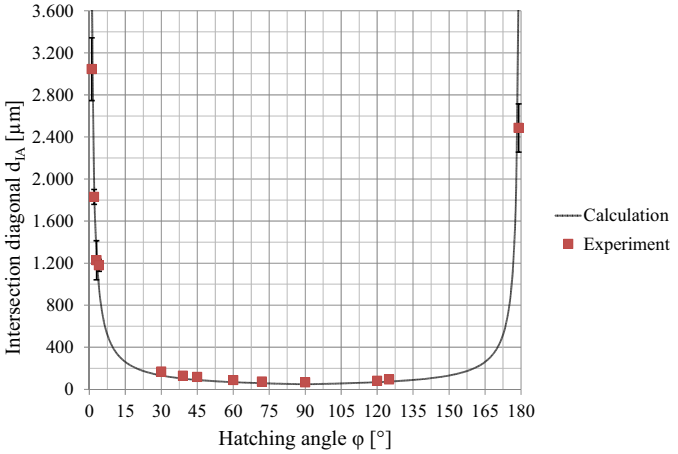

Fig. 4. Intersection diagonal depending on the hatching angle.

As the angular settings from $\varphi = 1° - 5°$ and from $\varphi = 175° - 179°$ show an identical behaviour in Figure 2 the the conclusion can be made, that the length of intersection diagonal and thus the size of intersection area significantly influences the formation of roughness. Scaling this relation to a larger context this means that during areal ablation a large number of intersections occur which each include a 1,8 − 2,0 times higher ablation depth in the intersection zone than in single laser tracks. These irregularities add up over the entire ablation area and thus create a roughness. Therefore the intersection diagonal is the characteristic parameter to explain elevated surface roughness at angles of $\varphi = 1° - 5°$ and $\varphi = 175° - 179°$ (Figure 10). Nevertheless increased roughness at angles between $\varphi = 6° - 174°$ cannot be explained through intersection diagonal and intersection area since the high exposed values from Figure 2 are not represented by the model curve and experiments from Figure 4.

4.3. Multiple track intersection

During areal ablation not only intersections between two laser vectors occur. When multiple layers are ablated the probability increases that an already existing intersection between two laser tracks is irradiated several times more. Therefore the objective of this experiment is to find the relationship between the number of multiple overlapping laser tracks and the depth of the resulting intersection area. Laser tracks are distributed around the circumference and crossed at one point (Figure 5a). The following quantity of tracks are examined: n = 2, 3, 4, 5, 8, 16, 32, 64 and 128 and the depth of the intersection areas is measured.

In Figure 5b an approximately linear relationship between the number of intersecting tracks and depth of the resulting intersection area is shown on a logarithmic scale. The linearity applies within the regarded range of ablated depth. For a bigger depth a decline of further ablation due to effects of radiation shielding and a limited aspect ratio can be assumed [18].

For areal ablation it can be derived that the shown increase in depth of multiple intersection areas leads to a corresponding increase in surface roughness. Nevertheless the appeareance of multiple track intersections during areal ablation is dependent on a statistical component (Figure 6) and in practice also dependent on the dimension of workpiece geometry. Therefore this mechanism cannot be directly related to certain angular settings. Yet the probability that points with an already present two-track intersection are irradiated several times more, increases with a smaller hatching angle, a smaller track distance and larger number of ablated layers (Figure 6). Additionally a mathematical precise point of multiple intersection is not neccesarry. Regarding the laser process it is sufficient when an almost intersection is present. In this case the laser focus passes the intersection area partially and the already present cavity from a previous intersection is further deepened due to the combination of small but deep cavities with effects of self focusing caused by reflections due to a non rectangular incidence angle when impacting a non planar surface [19].

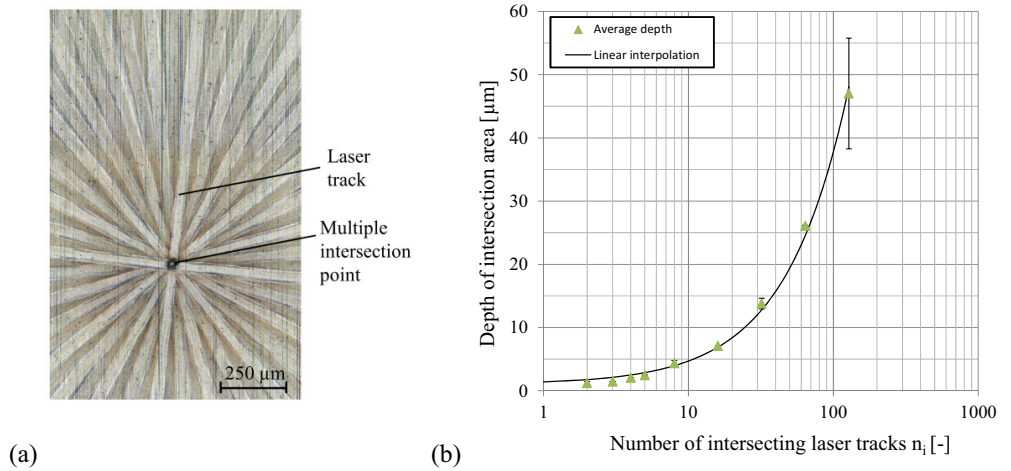

Fig. 5. (a) Microscopic image of multiple intersection; (b) depth of intersection depending on the number of intersecting laser tracks.

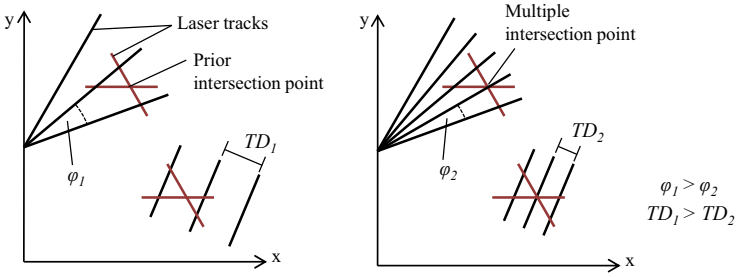

Fig. 6. Existence of multiple intersection point in dependency of hatching angle and track distance.

Therefore the presence of multiple track intersections can give an explanation for the scattering of roughness values for varying angles from Figure 2 that still are associated within the same mechanism of roughness formation (Figure 10). For the explanation of significantly elevated values of surface roughness in the midrange for hatching angles (e.g. $\varphi = 30°, 45°, 90°, 120°$ et cetera) further considerations need to be made.

4.4. Cycle completion number

In order to determine the formation mechanism behind increased roughness at angles between $\varphi = 6° - 174°$ the cycle completion number n_{cyc} is introduced. The cycle completion number describes after how many applied layers the laser tracks are identically orientated as the first layer depending on the hatching angle i.e. after how many layers a cycle is completed. Referring to the described symmetry (Section 3.3.) the forth or backwards moving direction of the laser focal spot (Figure 7a) has no influence on the passing behavior within a groovelike laser track. Accordingly angular settings of $\varphi = 0°$ and $\varphi = 180°$ are associated to a cycle completion number of $n_{cyc} = 1$ while for example $\varphi = 90°$ is related to $n_{cyc} = 2$ and $\varphi = 60°$ as well as $\varphi = 120°$ are in the same orientation after $n = 3$ layers. After a cycle is completed the groove of the first laser track of the cycle is further deepened and a regular, periodic profile of roughness is manifested (Figure 7b). In this context the number of passes n_{pas} describes the amount of passes of the the focal spot within an identical laser track until 360 layers of ablation are reached.

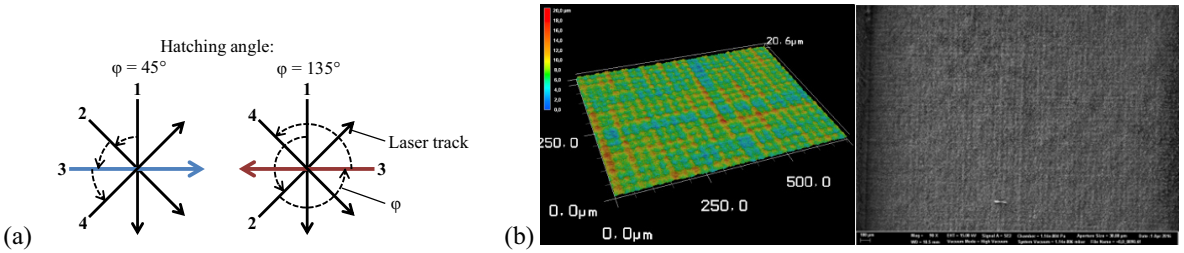

Fig. 7. (a) Scheme of forth or backwards direction of the laser; (b) Regular pattern in 3D-topography and SEM-image.

The model description for cycle completion number and number of passes is represented by the formula involving the least common multiple (LCM) (2).

$$n_{cyc} = \frac{LCM(180°,\varphi)}{\varphi} \quad \varphi \neq 0 \ , \qquad n_{pas} = \frac{360°}{n_{cyc}} \tag{2}$$

Figure 8 shows the calculated values of the cycle completion number and the number of passes in an identical laser track at $n = 360$ layers for all hatching angles between $\varphi = 0°$ and $\varphi = 180°$. Hatching angles that lead to a high roughness (compare Figure 2) are marked with red squares (Figure 8). Due to the correlation between the appearance of high roughness values and a low cycle completion number the conclusion can be made that a high number of passes in an identical laser track creates an increased surface roughness. Therefore increased roughness at angles between $\varphi = 6° - 174°$ can be explained by the cycle completion number.

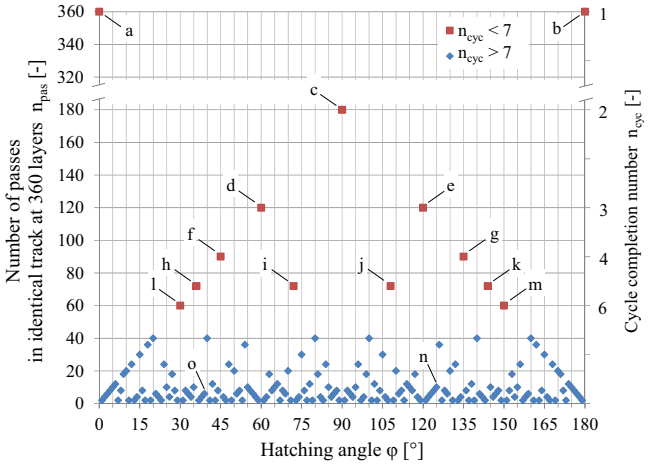

Point	Hatching angle φ [°]	Surface roughness S_a [µm]
a	0	2,91
b	180	1,33
c	90	1,21
d	60	1,09
e	120	1,36
f	45	1,06
g	135	0,98
h	36	0,95
i	72	1,00
j	108	0,99
k	144	1,01
l	30	1,04
m	150	0,96
n	125	0,84
o	39	0,87

Fig. 8. Cycle completion number and number of passes depending on the hatching angle.

4.5. Roughness development stages

The identified mechanisms of roughness formation are subsequently transferred to an areal ablation process where three different hatching angles $\varphi = 3°, 42°, 90°$ are examined. Objective of the experiment is to investigate the development of surface roughness for the three hatching angles and to connect them with the prior identified mechanisms of surface roughness formation. Therefore in each case $n = 5, 15, 25, 60, 120, 180, 240, 300, 360$ layers are ablated and the roughness S_a is measured at each stage. The choice of hatching angles in combination with the number of layers ensures that more than a full cycle is completed ($n_{cyc,\ 3°} = 60$, $n_{cyc,\ 42°} = 30$, $n_{cyc,\ 90°} = 2$) and the roughness values therefore reach their peak level.

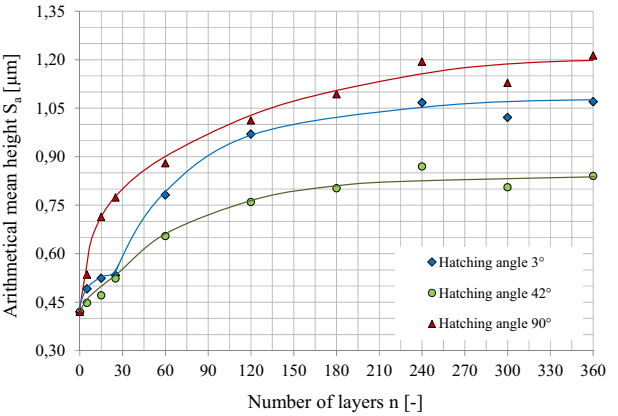

Fig. 9. Development stages of surface roughness.

As for all other experiments ablation begins on a tungsten carbide blank with a surface roughness of $S_a = 0{,}42$ µm. Figure 9 shows that the surface roughness increases layer by layer until it reaches its maximal value dependent on the hatching angle. The overall trend shows that the roughness initially increases quickly for all hatching angles and subsequently each maximum value of roughness is reached asymptotically.

At a hatching angle of $\varphi = 90°$ the surface roughness increases strongly within the first 15 layers due to the formation of a regular, periodic profile. The mechanism of surface roughness formation based on the cycle completion number is dominant (see Figure 8). In contrast at a hatching angle of $\varphi = 3°$ the formation of a regular, periodic profile is not present. The formation of roughness is based on the mechanism of intersection areas. For this reason the roughness increases slowly at first while the rate of increase rises after $n = 30$ layers when a larger number of intersections has been generated. With a hatching angle of $\varphi = 42°$ a final roughness of $S_a = 0{,}84$ µm is created which stays on a level lower than with hatching angles of $\varphi = 3°$ and $\varphi = 90°$. In the case of a $\varphi = 42°$ hatching angle the mechanism of intersection areas also influences the resulting surface quality. Yet the influence does not lead to an elevated roughness due to the presence of only small intersection areas (see Figure 4). Furthermore the formation of a regular, periodic profile is excluded by a cycle completion number of $n_{cyc,\ 42°} = 30$.

5. Conclusion

In the presented research the influence of the hatching exposure strategy on the surface quality during picosecond laser ablation of tungsten carbide was examined. Two significant mechanisms of roughness formation were identified which both contribute to a high value of surface roughness. While the intersection diagonal d_{IA} and the corresponding intersection area A_{IA} are the characteristic parameters to explain elevated surface roughness at angles of $\varphi = 1° - 5°$ and $\varphi = 175° - 179°$, the cycle completion number n_{cyc} determines increased roughness at angles between $\varphi = 6° - 174°$ as well as for $\varphi = 0°$ and $\varphi = 180°$ (Figure 10). In conclusion guidelines are derived which present a favorable setting for a laser ablation process of high quality. The following boundary conditions should be taken into account during a high quality laser ablation process:

- Choosing hatching angles over $\varphi = 5°$ but below $\varphi = 175°$ in order to receive a small intersection area, ideally the parameter of intersection diagonal should be within $d_{IA} < 200$µm presumed similar laser parameters, especially a similar width of laser track, are used.
- At the same time choosing hatching angles with a high cycle completion number, ideally $n_{cyc} > 7$.

- Adjustment of hatching angle in such a way that multiple track intersections are avoided. This can be achieved by large hatching angles and a large track distance TD, given that conformity with the determination of laser parameters is ensured.
- As exemplary by a setting of possible hatching angles of $\varphi = 39°$, 42° or 125° an elevation in roughness can be avoided.

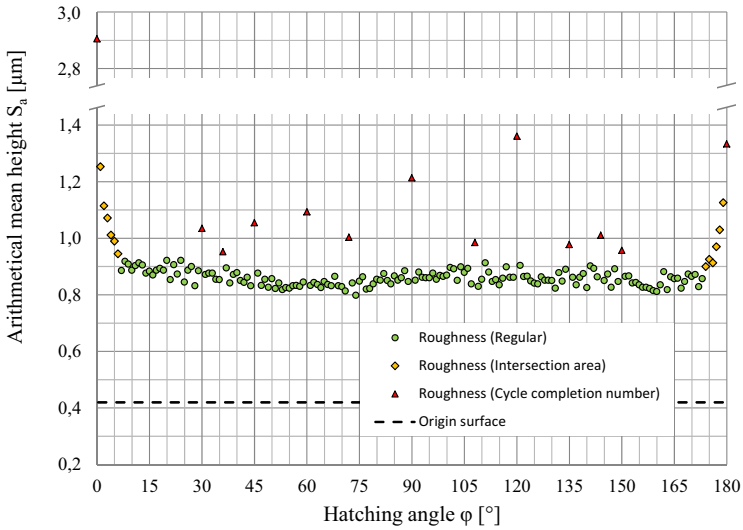

Fig. 10. Classification for mechanisms of surface roughness formation.

By complying to the discussed guidelines in the present examination the surface roughness can be reduced from a value of $S_a = 2{,}9$ in the worst case of applying a hatching angle of $\varphi = 0°$ to $S_a = 0{,}84$µm with a hatching angle of $\varphi = 42°$. Also other hatching angles fulfill the boundary conditions and reach comparable results like $S_a = 0{,}84$ µm with a hatching angle of $\varphi = 77°$. With this approach the initial roughness can be reduced by factor 2,0 − 3,5 with very low consumption of time and effort by simply setting a favorable hatching angle. Therefore applying a hatching angle represents a feasible possibility for industrial ablation processes without integration of any additional, complex or expensive systems. Furthermore due to the identification of roughness formation as a geometrically based effect, it can be assumed that the examined mechanisms can also be transferred to ablation processes with different types of materials and laser sources.

References

[1] Dold, C., Henerichs, M., Bochmann, L., Wegener, K., 2012. Comparison of ground and laser machined polycrystalline diamond (PCD) tools in cutting carbon fiber reinforced plastics (CFRP) for aircraft structures., 5th CIRP Conference on High Performance Cutting 2012, Procedia CIRP1, 2012, 178 – 183.

[2] Hallmann, S., Nodop, .R., Daniel, C., Weppler, M., Geis-Gerstorfer, J., Emmelmann, C., 2015. Improvement of the adhesion between CoCr and dental ceramics by laser surface structuring, Lasers in Manufacturing Conference 2015.

[3] Kordt, J., 2007. Konturnahes Laserstrahlstrukturieren für Kunststoffspritzgießwerkzeuge. Hochschulverlag RWTH Aachen.

[4] Hallmann, S., Glockner, P., Daniel, C., Seyda, V., Emmelmann, C., 2015. Manufacturing of Medical Implants by Combination of Selective Laser Melting and Laser Ablation, Lasers Manuf. Mater. Process., Springer New York 2015.

[5] Walter, C., Komischke, T., Weingärtner, E., Wegener, K., 2014. Structuring of CBN grinding tools by ultrashort pulse laser ablation., 6th CIRP International Conference on High Performance Cutting, HPC2014., Procedia CIRP 14, 2014, 31 – 36.

[6] Oberg, E., Jones, F., Horton, H., Ryffel, H., 2012. Machinery's Handbook 29th Edition, Industrial Press, New York, 2012.

[7] Daniel, C., Ostendorf, S., Hallmann, S., Emmelmann, C., 2016. Picosecond laser processing of polycrystalline cubic boron nitride. Journal of Laser Applications 28, 012001.

[8] Eberle, G., Wegener, K., 2014. Ablation Study of WC and PCD Composites Using 10 Picosecond and 1 Nanosecond Pulse Durations at Green and Infrared Wavelengths, 8th International Conference on Photonic Technologies LANE 2014, Physics Procedia, 2014, 56, 951-962.
[9] Neuenschwander, B., Jaeggi, B., Schmid, M., Hennig, G., 2014. Surface structuring with ultra-short laser pulses: Basics, limitations and needs for high throughput, 8th International Conference on Photonic Technologies LANE 2014, Physics Procedia, 2014, 56, 1047 – 1058.
[10] Campanelli, S., Casalino, G., Contuzzi, N., Ludovico, A., 2013. Taguchi optimization of the surface finish obtained by laser ablation on selective laser molten steel parts., 8th CIRP Conference on Intelligent Computation in Manufacturing Engineering, Procedia CIRP12, 2013, 462 – 467.
[11] Koch, J., Schaaf, P., Rädlein, E., 2011. Laserendbearbeitung metallischer Werkstoffe. Universitätsverlag Ilmenau, 2011.
[12] Rosa, B., Mognol, P., Hascoet, J.Y., 2015. Laser polishing of additive laser manufacturing surfaces, Journal of Laser Applications, Band 27, Nr. S29102, 2015.
[13] Temmler, A., Willenborg, E., Wissenbach, K., 2011. Design Surfaces by Laser Remelting. Physics Procedia, Band 12, S. 419-430, 2011.
[14] Schulze, V., Weber, P., 2010. Precise ablation milling with ultra short pulsed Nd:YAG lasers by optical and acoustical process control. Laser-based Micro- and Nanopackaging and Assembly IV, Proc. of SPIE Vol. 7585, 2010.
[15] Neef, A., Seyda, V., Herzog, D., Emmelmann, C., Schönleber, M., Kogel-Hollacher, M., 2014. Low Coherence Interferometry in Selective Laser Melting., 8th International Conference on Photonic Technologies LANE 2014, Physics Procedia, Band 56, S. 82-89, 2014.
[16] Meijer, J., Du, K. Gillner, A., Hoffmann, D., Kovalenko, S., Masuzawa, T., Ostendorf, A., Poprawe, R., Schulz, W., 2002. Laser Machining by Short and Ultrashort Pulses, State of the Art. CIRP Annals - Manufacturing Technology, Volume 51, Issue 2, 2002, S. 531–550.
[17] Klocke, F., König, W., 2008. Fertigungsverfahren Drehen, Fräsen, Bohren, Springer, Berlin, 2008.
[18] Kaakkunen, J., Silvennoinen, M., Paivasaari, K., Vahimaa, P., 2011. Water-Assisted Femtosecond Laser Pulse Ablation of High Aspect Ratio Holes. LiM 2011, Physics Procedia 12, 2011, 89–93.
[19] Stafe, M., Marcu, A., Puscas, N., 2014, Pulsed Laser Ablation of Solids, Basics, Theory and Applications., Springer, Berlin, 2014.